



Microkinetic modelling for selective catalytic reduction (SCR) of NO_x by propane in a silver-based automotive catalytic converter

B. Sawatmongkhon^a, A. Tsolakis^{a,*}, K. Theinnoi^b, A.P.E. York^c, P.J. Millington^c, R.R. Rajaram^c

^a School of Engineering, Mechanical and Manufacturing Engineering, University of Birmingham, Birmingham B15 2TT, UK

^b College of Industrial Technology, King Mongkut's University of Technology North Bangkok, Bangkok, Thailand

^c Johnson Matthey Technology Centre, Blount's Court, Sonning Common, Reading RG4 9NH, UK

ARTICLE INFO

Article history:

Received 29 July 2011

Received in revised form

19 September 2011

Accepted 25 September 2011

Available online 29 September 2011

Keywords:

HC-SCR

Ag/Al₂O₃

Emissions

Modelling

ABSTRACT

A numerical simulation is designed in order to better understand the selective catalytic reduction of NO_x by propane (C₃H₈-SCR) in the presence of hydrogen. The simulation was designed for a single channel of a monolith typical for automotive catalytic converters, coated with a silver alumina catalyst (Ag/Al₂O₃). The complicated physical and chemical processes occurring during the reactions are solved by computational fluid dynamics (CFD) coupled with a surface-reaction mechanism. This mechanism is developed based on detailed microkinetic analysis. The elementary-step-like surface reaction mechanism (consisting of 94 reactions, 24 gas-phase species and 24 adsorbed surface species) is applied to investigate the effect on the conversion of NO_x to N₂ of chemical kinetic steps, such as intermediate species. Results from the modelling emphatically agree with the experimental data. The modelling can predict the NO_x conversion at various operating conditions. Furthermore, the modelling can also provide information that is difficult to measure, for example predicts the channel wall temperature and surface coverage of surface species.

© 2011 Elsevier B.V. All rights reserved.

1. Introduction

Measurement of physical and chemical properties and processes in the small (e.g. diameter <1 mm) channels of honeycomb catalytic converters is cumbersome and difficult. Computer simulation can provide an understanding of the physical and chemical details that occur in an after treatment process. To simulate the performance of an after treatment system, knowledge about physical properties of fluid flow inside a catalytic converter (e.g. velocity, temperature profiles, density and viscosity) and chemical phenomena on the catalyst surface and/or in the gas-phase (e.g. reaction rate, intermediate species and heat of reaction) is necessary.

To provide information about the rate at which a chemical process takes place, different rate expressions have been suggested in literature. A power law rate expression has regularly been used in a gas phase reaction, also called homogeneous reaction, as well as catalytic reaction. Constant values appeared in this rate expression are normally extracted from experimental data. Since the catalytic reaction occurs on the limited catalyst surface, the rate of reaction is decreased when free active sites are decreased. However,

the rate expression formed by the power law does not include the effect of the catalyst active sites availability on the rate of reaction, resulting in validity over a limited range of operating conditions. Moreover, the power law rate expression needs a lot of experiments to determine constant values. To capture the effect of catalyst surface state, the Langmuir–Hinshelwood–Hougen–Watson (LHHW) rate expression originally based on Langmuir adsorption has been systematically developed and successfully implemented to many catalytic reaction applications. Nevertheless, LHHW reaction model requires few assumptions such as a rate-determining step (RDS), most abundant reaction intermediate (MARI), quasi-steady state (QSS) and partial equilibrium (PE). In many applications that involve catalytic reaction, the rate-determining step changes when the operating condition is changed. Therefore, the validity of these assumptions cannot be verified. Like the power law rate expression, LHHW method requires the input of several data from experiments for model discrimination and parameter estimation [1,2].

Microkinetic analysis is an examination of catalytic reactions in terms of elementary chemical reactions that occur on the catalytic surface and their relation with each other and with the surface during a catalytic cycle [3]. The aim of the microkinetic approach to a gas/solid catalytic reaction is to correlate the kinetic parameters from both experimental data and theoretical principles for surface elementary steps (adsorption, desorption, Langmuir–Hinshelwood steps) involved in a plausible mechanism of the reaction [3].

* Corresponding author. Tel.: +44 0 121 414 4170; fax: +44 0 121 414 7484.

E-mail address: a.tsolakis@bham.ac.uk (A. Tsolakis).

Nomenclature

A_k	pre-exponential factor of elementary reaction k (s^{-1})
C_p	specific heat at constant pressure, J/(kg K)
c_j	concentration of species j , (mol/m ³)
$D_{i,B}$	diffusion coefficient of species i diffusing in the mixture of i and B (m ² /s)
E_a	activation energy, (kJ/mol)
h_i	enthalpy of species i , (kJ/kg)
J	diffusive mass flux, kg/(m ² s)
K_s	number of surface reactions
k_k	reaction rate coefficient of elementary reaction k
M_i	molecular weight of species i , (kg/kmol)
N_g	number of gas-phase species
N_s	number of surface species
n	reaction order
P	pressure (Pa)
R	universal gas constant, kJ/(kmol K)
R_i	net rate of production of species i due to chemical reactions
r	radial spatial coordinate (m)
S_i^0	sticking coefficient at vanishing coverage of species i
\dot{s}_i	surface reaction rate of species i , mol/(m ² s)
T	temperature (K)
v_r	radial velocity (m/s)
v_z	axial velocity (m/s)
Y_i	mass fraction of species i (kg/kg)
z	axial spatial coordinate (m)

Greek symbols

β	temperature exponent
Γ	site density (kmol/m ²)
λ	thermal conductivity, W/(m K)
μ	viscosity, (Pa s)
ν'	stoichiometric coefficient for the reactants
ν''	stoichiometric coefficient for the products
ρ	mass density (kg/m ³)

Indices

i	species number
k	elementary reaction number
r	in radial direction
z	in axial direction

Selective catalytic reduction of NO_x with hydrocarbons (HC-SCR) as reductants has been extensively researched and developed as a potential method for the removal of NO_x under oxygen-rich conditions. Among, the many HC-SCR catalysts that were tested under laboratory and real engine exhaust conditions, silver (Ag) had been widely accepted as the most promising catalyst for practical applications. Silver catalysts show excellent ability in reduction of NO_x using a wide variety of species, such as, oxygenated hydrocarbons [4,5], light hydrocarbons [6,7] and heavy hydrocarbons [8,9].

When silver-based catalysts are used, high exhaust temperatures are required for good NO_x reduction efficiencies, and a major drawback of silver catalysts is their lack of low temperature activity. Although, their activities can be improved at low temperatures when long chain hydrocarbons are used [10,11], this is not enough to achieve acceptable catalyst activity unless hydrogen is present. Hydrogen is widely considered as an ideal

co-feeder gas in active mode (i.e. injected HCs) HC-SCR operation in order to decrease the minimum temperature needed to drive the NO_x-reducing reactions. Shimizu and co-workers proposed that hydrogen kinetically promotes several chemical processes in HC-SCR over Ag catalysts: (1) oxidation of NO to nitrate [12–14]; (2) oxidation of NO to NO₂ [9,12–14]; (3) partial oxidation of hydrocarbon to acetate [12–14]; (4) oxidation of hydrocarbon to CO_x [15]; (5) oxidation of acetate with NO + O₂ mixture [12,13]; (6) enhancement of rate-determining step [13,14] and (7) prevention active sites from strongly adsorbed species, such as nitrates, at low temperature [9,15,16]. Shibata et al. found that the addition of hydrogen leads to the remarkable promotion of hydrocarbon to mainly surface acetate, which is the rate-determining step of HC-SCR in the absence of hydrogen [13]. Later, Shimizu et al., after conducting some kinetic studies, reported that hydrogen addition results in a decreased activation energy for NO_x reduction (i.e. the temperature window was shifted towards lower values) [15]. They also showed that the addition of hydrogen can retard nitrate poisoning by reducing the concentration of nitrates on the catalyst surface, therefore, leading to enhancing the HC-SCR reaction dramatically. This preventive effect was also reported currently by Creaser et al. [16]. Sazama et al. studied the enhancement of decane-SCR by hydrogen over an Ag/Al₂O₃ catalyst. They published that the transformation of intermediate cyanide species, bound on Ag⁺ site, into isocyanate, bound on Al site, and oxidation of decane to formate are the surface reaction steps that are substantially elevated by the promotion of hydrogen [14]. By in situ UV–vis spectroscopic analysis, the addition of hydrogen reduces Ag⁺ ions that are normally observed in the absence of hydrogen and produces moderately agglomerated Ag_n^{δ+} clusters that promote the NO_x reduction activity generally through the activation of the hydrocarbon [12,14]. Shimizu et al. reasonably assumed that the addition of hydrogen results in the formation of hydride on silver clusters, which may react with oxygen to form a reactive oxidant, such as hydroperoxy radical (HO₂), peroxide (O₂^{2−}) or superoxide ions O₂[−] [15]. Houel et al. suggested that the addition of hydrogen promotes the formation of NO₂ over the Ag/Al₂O₃ catalyst, which is very effective in oxidising carbon-rich species harmfully formed on the catalyst surface when diesel fuel or long chain hydrocarbons (>C₁₂) are used as reductants, accordingly preventing catalyst deactivation at low temperatures and allowing high NO_x conversion to be maintained [9]. In the presence of H₂, Zhang et al. found gas-phase acetaldehyde and acrolein as partial oxidation products of C₃H₆ and gas-phase nitrogen-containing products such as nitromethane. However, these gas-phase products could not be detected in the absence of H₂ [17]. On the other hand, Wichterlová et al. studied the effect of H₂ and CO during the SCR of NO_x over an Ag/Al₂O₃ catalyst by in situ UV–vis and FTIR spectroscopy techniques. They found that the formation of Ag_n^{δ+} clusters was observed in both H₂ and CO as the co-reductants but the promotion of NO_x reduction was found only in the case of H₂. They concluded that the promotional effect of H₂ on the NO_x reduction activity at low temperature did not relate to the formation of Ag_n^{δ+} clusters. However, they also suggested that hydrogen itself participates in the NO_x reduction processes with a chemical function resulting in the acceleration of critical SCR-NO_x elementary steps [18].

In order to further promote the chemical reactions of NO_x-SCR by hydrocarbons, an understanding of the HC-SCR process at the molecular level is necessary. In the present work, a novel surface-reaction mechanism for C₃H₈-SCR is set up with emphasis on microkinetic analysis aiming to investigate the chemical behaviour during the process at a molecular level via detailed elementary reaction steps.

In this work, we designed the model under the hypothesis that the presence of hydrogen changes the state of the Ag/Al₂O₃ catalyst, and so does not chemically react with any other gas-phases or

Table 1
Monolith specification.

Parameter	Unit	Value
Length	mm	25
Diameter	mm	24
Support		Cordierite
Cell shape		Square
Cell density	cpsi	400
Wall thickness	mm	0.152
Washcoat thickness	mm	0.025
Hydraulic diameter	mm	1.068
Open frontal area	%	70.72
Geometric surface area	m ² m ⁻³	2649

surface species. The mechanism has been validated and optimised by comparison with experimental data.

2. Experimental

A silver catalyst 2 wt.% (supplied by Johnson Matthey Plc) was prepared by impregnating γ -alumina (surface area 150 m²/g) with aqueous AgNO₃ before drying and calcining in air for 2 h at 500 °C. The catalyst was made into an aqueous suspension, which was then uniformly coated onto ceramic monolith substrates with cell density 400 cpsi. The dimensions, given as diameter \times length, of the catalyst used for the experiments were 24 mm \times 25 mm with a wall thickness 0.152 mm. The specifications of the monolith are summarised in Table 1. The monolithic catalyst was installed in a quartz-tube reactor; then, heated by a tubular furnace. Its temperature was monitored through a thermocouple positioned at the inlet of the reactor, 5 mm upstream of the catalyst bed. A simplified schematic of the monolithic reactor system used is shown in Fig. 1.

Gas compositions at the inlet of reactor were generated by high purity bottled gases and controlled by metering valves. The compositions of gases at the inlet of the reactor were 2000–4000 ppm total hydrocarbon (THC), 200–600 ppm NO₂, 12% O₂, 0% H₂O, 0% CO₂, 0 ppm CO and N₂ (balance) at 15 L/min (80,000 h⁻¹ space velocity). All of the tests were performed with 600 ppm hydrogen addition from a certified bottled source with a high purity (>99%). The exhaust temperatures at the inlet of the reactor were

Table 2
Experimental conditions.

Experimental condition	Inlet temperature (°C)	Inlet THC (ppm)	Inlet NO (ppm)
1	250	1758	200
2	250	2111	418
3	250	2116	601
4	250	4135	202
5	250	4287	395
6	250	4253	604
7	290	1719	198
8	290	1841	399
9	290	1892	626
10	290	3934	209
11	290	3982	403
12	290	4027	603
13	370	2146	197
14	370	2104	413
15	370	2250	597
16	370	4007	199
17	370	3912	416
18	370	3911	605

250–370 °C (controlled by the furnace). All experimental conditions are detailed in Table 2.

A Horiba Mexa 7100DEGR analyser was employed to measure the concentrations of NO_x, CO, CO₂, O₂ and THC. The Horiba measures NO_x (NO + NO₂) by chemiluminescence, CO and CO₂, are measured using non-dispersive infrared (NDIR), O₂ by an electrochemical method and hydrocarbons by flame ionisation detection (FID).

3. Development of a C₃H₈-SCR microkinetic mechanism

A microkinetic mechanism of C₃H₈-SCR on a silver catalyst is constructed based on the hierarchical multiscale approach which was originally developed by Vlachos research group [19]. Chemically mechanistic understanding of HC-SCR such as intermediate surface species is taken from the literature; then, all possible elementary reaction steps are formed. Activation energies and heats of reaction are determined through heats of adsorption that can be calculated by using the theory of unity bond index-quadratic exponential potential (UBI-QEP), the theory originally established by Shustorovich and co-workers [20–22]. Pre-exponential factors are estimated by order of magnitude obtained from transition state theory (TST). Sensitivity analysis (SA) is applied in order to identify the important elementary reaction steps of C₃H₈-SCR mechanism. Finally, pre-exponential factors of these reaction steps are optimised via the solution mapping method to fit simulated results with data from experiments.

3.1. Reaction pathways

In the partial oxidation of propane and propylene on mixed metal oxide catalysts, as described in a review work by Bettahar et al. [23], i-propanol was found as the intermediate product of propane.

Nitrates (NO₃) are considered as one of the most crucial intermediates in the initial stage of the HC-SCR reaction. The accumulation on a catalyst surface of nitrates proceeds by oxidation of NO to NO₂ then adsorption of NO₂ on surface oxygen species [24]. Monodentate, bidentate and bridging are general types of nitrate which are found as surface species during HC-SCR processes. Kameoka et al. studied the role of surface nitrates by in situ diffuse reflectance infrared Fourier transform (DRIFT) spectroscopy and temperature-programmed desorption (TPD) techniques. They reported that the reactivity with organic nitro compounds to form surface isocyanate

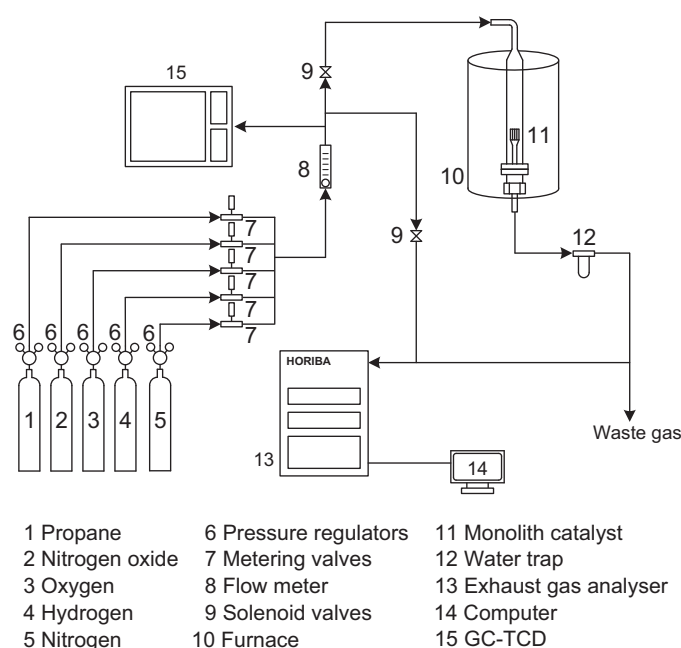


Fig. 1. A simplified schematic of the catalyst test rig.

species of the monodentate nitrate is higher than that of the bidentate and bridging nitrate [25]. Furthermore, they also found that adsorbed NO and NO₂ were hardly observed on the surface of catalyst. At high NO concentration or low temperature, nitrates act like inhibitor in NO_x reduction activity by strongly adsorbing on the catalyst surface [26].

Acetaldehyde was usually found as the intermediate species in the selective reduction of NO_x by using oxygenate hydrocarbon as a reducing agent [27–33]. In ethanol-SCR acetaldehyde is formed by the reaction of ethanol with O₂ and/or NO₂; then it is oxidised to form acetate [32]. Furthermore, acetaldehyde was also observed in the propene(C₃H₆)-SCR with the promotion of hydrogen on Ag/Al₂O₃ catalyst [17].

Produced via the partial oxidation of hydrocarbon, acetate is generally considered as the key intermediate surface species in a selective reduction of NO_x over Ag/Al₂O₃ catalysts [6,24,26,34,35]. Nevertheless, acetate is rarely activated by NO or O₂, but is easily consumed in a NO + O₂ mixture, probably nitrates [26]. Shimizu et al. found that the consumption rate of acetate in a mixture of NO and O₂ showed the same order of magnitude as the conversion rate of NO to N₂. Therefore they summarised that acetate was active as a reductant and took part in the N₂ formation through the reaction with a NO + O₂ mixture, possibly nitrates [6]. Moreover, Shibata et al. suggested that, in case of Ag/Al₂O₃ catalyst, the formation of surface acetate (derived from partial oxidation of various hydrocarbons by oxygen) is the rate-determining step for C₃H₈-SCR, regardless of the promoting effect by hydrogen [13].

In the selective catalytic reduction of NO_x, isocyanate (NCO) and cyanide (CN) are widely accepted as key intermediates in HC-SCR [26,34,36–38]. The formation of isocyanate species is believed to form from stored surface N-containing species (probably nitrate) and stored surface C-containing species (probably acetate) [26,38]. Moreover Bion et al. studied the formation of isocyanate from the reaction between isotope C¹⁸O and N¹⁶O and concluded that on Ag/Al₂O₃ isocyanate species are not formed by linkage of CO molecules to surface nitrogen species due to the dissociation of NO [37]. In terms of the consumption of isocyanate, three possible paths have been proposed; (1) isocyanate species are consumed by O₂ [26,36], (2) consumed by a mixture of NO and O₂ [26,36] and (3) consumed by water, hydrolysis process [37,38]. Kameoka et al. investigated the effect of silver and the reactivity of surface isocyanate species over Ag/Al₂O₃ and Al₂O₃ catalysts on the conversion of NO_x to N₂ [36]. The reaction of surface isocyanate with O₂ proceeded only in the presence of silver, while reacted with a mixture of NO and O₂ (possibly NO₂) both in the presence and absence of silver. Interestingly, over Ag/Al₂O₃ catalysts, the total amount of N₂ formation almost equalled the summation of two surface reactions; (1) the reaction between surface isocyanate and O₂ occurring on silver sites and (2) the reaction of surface isocyanate with NO + O₂ existing on Al₂O₃ sites. Furthermore the reaction rate of the former is higher than the latter; this indicates that the most parts of surface isocyanate species are consumed by O₂ on silver sites. On the other hand, surface isocyanate species were rapidly consumed by water, to produce gas-phase ammonia (NH₃) and CO₂. Ammonia, then, reacts rapidly with gas-phase NO_x or surface nitrates (and nitrites) to produce N₂ [37,38]. Yeom et al. studied ethanol-SCR of NO_x over various silver based catalysts. By isotropic experimental technique, they found that most of the carbon atoms in the isocyanate come from the methyl carbon of ethanol [32].

In terms of surface cyanide species, Bion et al. have concluded that cyanide species are the precursor of isocyanate [37]. Cyanide species are derived from hydrocarbon, ethanol in this case, then isomerised to surface isocyanides after that reacted by oxygen to form surface isocyanate. Cyanide also is quickly converted to isocyanate by reacting with water on a Ag/γ-Al₂O₃ catalyst [32].

Mhadeshwar et al. [39] proposed the mechanism of HC-SCR by using both intermediate species and reaction pathways based on ethanol-SCR; first, all types of hydrocarbons are oxidised to ethoxy radical. Then, ethoxy radical is split into two major pathways; one oxidise to acetaldehyde and another one to ethylene. Ethylene is oxidised to carbon dioxide; however, acetaldehyde is used as a reducing agent in order to convert NO to N₂. In this paper, the pathway of the C₃H₈-SCR on a silver based catalyst is shown in Fig. 2. Two main chemical reaction pathways of HC-SCR are complete oxidation of hydrocarbons and selective reduction of NO_x by oxygenated species that are produced from such hydrocarbons. On the basis of complete oxidation pathway, methoxy radical which is variously derived from i-propoxy radical, acetate and acetyl radical is the essential intermediate species for this process. Methoxy radical can be oxidised by oxygen to generate water vapour directly. Along with water vapour formation, carbon dioxide is indirectly produced from methoxy radical via formyl radical. In terms of selective reduction of NO_x route, nitromethane is the first intermediate which contain both carbon and nitrogen species. Nitromethane is created by either the reaction between surface acetate and nitrogen dioxide or the reaction of surface acetyl radical and nitrate. Both surface acetate and acetyl radical are derivative products that generate from the same source, acetaldehyde. Acetaldehyde appears as the surface intermediate species which is produced from propane by oxidation processes via i-propanol and i-propoxy radical species. Once nitromethane is formed, it is further chemically converted to nitrogen through nitromethylene, formaldiminoxy, nitrile N-oxide, cyanide and isocyanate respectively. The detailed elementary reaction mechanism for C₃H₈-SCR on a silver catalyst is presented in Table 3.

3.2. Parameter estimation

To estimate parameters of elementary reaction step based on microkinetic analysis, initial input variables are required: (1) site density, (2) sticking coefficients or pre-exponential factors, (3) temperature exponents, (4) surface bonding geometry, (5) bond dissociation energies and (6) heats of adsorption. The site density is adopted to be 1.66058×10^{-8} kmol/m² (10^{15} sites/cm²) [39]. Nitrogen is widely known as an inert gas which very low reactivity at low temperature; so the sticking coefficient for the adsorption of nitrogen, R(13), is zero. Recently, Mhadeshwar et al. [39] concluded from experience in SCR testing that CO₂ does not promote or inhibit the NO_x conversion. Therefore, the value of zero is applied for the adsorption of carbon dioxide, R(3). Unity is assumed for all remaining sticking coefficients. The pre-exponential factors are initially estimated by order of magnitude based on TST [3]. All temperature exponents are set by value of zero. Based on UBI-QEP theory, heats of adsorption are calculated via chemical knowledge about the surface bonding geometry combining with bond dissociation energies [40]; afterwards activation energies are computed from these heats of adsorption. The details about the calculation for heats of adsorption and activation energies are clearly explained by Storsæter et al. [41].

3.3. Parameter optimisation

The conversions of propane as well as NO_x and the ratio of carbon dioxide to carbon monoxide are selected as optimisation targets. Sensitivity analysis is applied to find the important pre-exponential factors that significantly affect the corresponding change in optimisation targets. The pre-exponential factor of each reaction is varied in each direction by one order of magnitude from an initial value. Sensitivity analysis indicates that optimisation targets are markedly influenced by 10 from 94 elementary

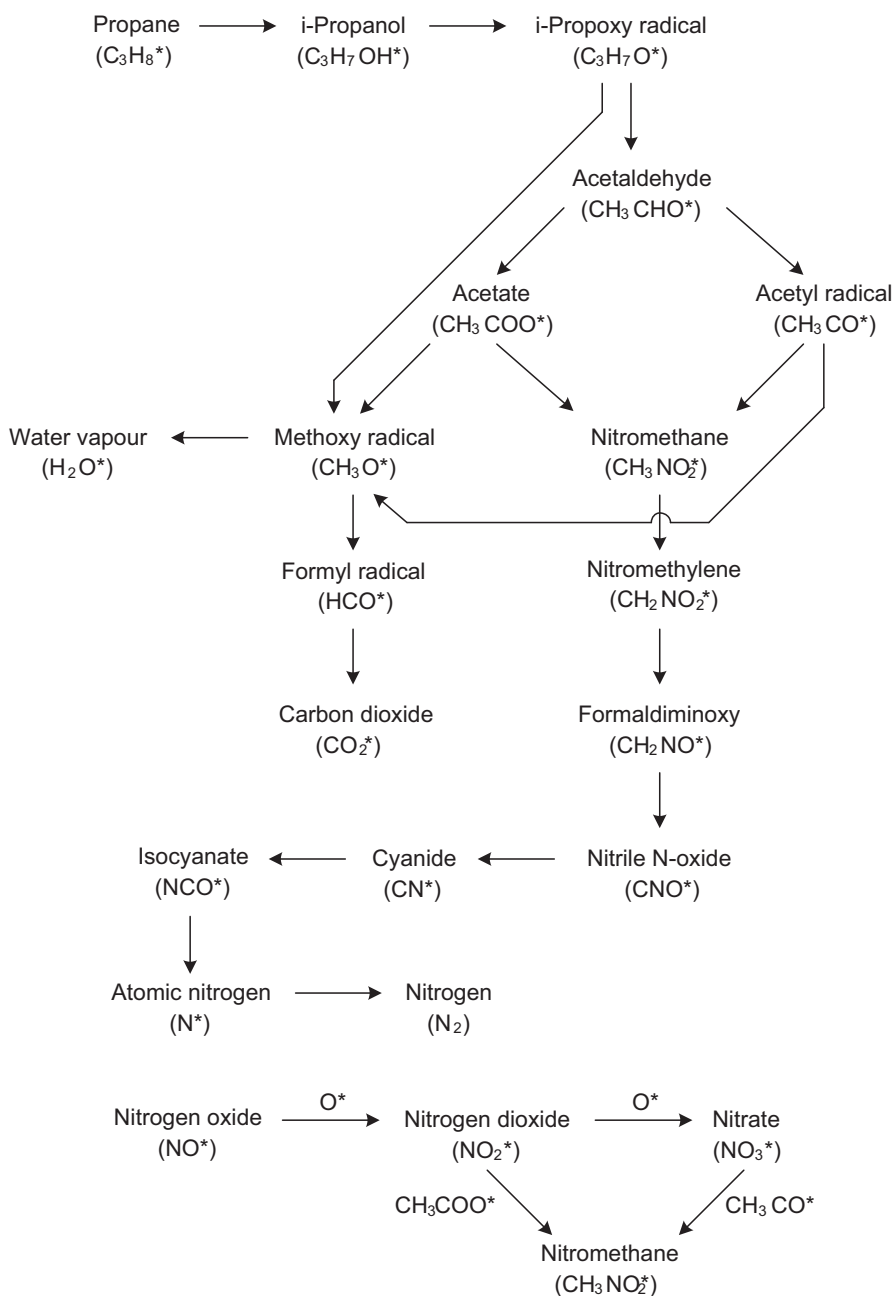


Fig. 2. Chemical reaction pathways of selective catalytic reduction of NO_x by propane.

reactions. The elementary reactions that are responsible for the conversion of propane conversion are R(16) and R(55). On the subject of the NO_x conversion, the primary objective, this optimisation target is controlled by R(15), R(16), R(59), R(63), R(73), R(75) and R(77). Regarding the ratio of carbon dioxide to carbon monoxide, the elementary reaction R(67) and R(91) control this ratio.

The solution-mapping method is one of methods used to determine an optimum set of parameters for multi-parameter multi-data-set optimisation. This method was originally used by Frenklach et al. [42] to form optimised parameters for a methane combustion mechanism. Aghalayam et al. [43] applied a solution-mapping method coupled with factorial design to optimise pre-exponential factors of catalytic hydrogen oxidation mechanism on platinum.

To capture the state of the catalytic surface which vary with operating condition along the reacting wall, Koop and Deutschmann [44] employed the dependence of pre-exponential factors in the form of modified Arrhenius expression. This expression takes a coverage dependence of a reaction rate through coverage-dependent activation energy parameter and coverage-dependent reaction order parameter. Similarly, to catch the considerable change of activation energies with varying operating conditions, Mhadeshwar and Vlachos [45] incorporated temperature and coverage dependence of activation energy by employing temperature and coverage dependence in the heat of chemisorption. In this paper, to realise the effect of operating conditions, some pre-exponentials are written as a function of temperatures and concentrations of propane and NO_x at inlet. Optimised pre-exponentials as a function of inlet conditions are listed in Table 4.

Table 3

Detailed reaction mechanism for C₃H₈-SCR on a silver catalyst with initial values of pre-exponential factor or sticking coefficient.

Reaction	Pre-exponential (s ⁻¹) or sticking coefficient	E _a (kJ/mol)
R(1) CH ₃ CHO + * → CH ₃ CHO*	1.0	0.00
R(2) CH ₃ CHO* → CH ₃ CHO + *	1.0 × 10 ¹³	43.25
R(3) CO ₂ + * → CO ₂ *	0.0	0.00
R(4) CO ₂ * → CO ₂ + *	1.0 × 10 ¹³	13.47
R(5) H ₂ O + * → H ₂ O*	1.0	0.00
R(6) H ₂ O* → H ₂ O + *	1.0 × 10 ¹³	35.76
R(7) O ₂ + 2* → 2O*	1.0	0.00
R(8) 2O* → O ₂ + 2*	1.0 × 10 ⁸	39.55
R(9) H ₂ + 2* → 2H*	1.0	0.00
R(10) 2H* → H ₂ + 2*	1.0 × 10 ¹³	19.77
R(11) C ₃ H ₈ + * → C ₃ H ₈ *	1.0	0.00
R(12) C ₃ H ₈ * → C ₃ H ₈ + *	1.0 × 10 ¹³	41.02
R(13) N ₂ + 2* → 2N*	0.0	0.00
R(14) 2N* → N ₂ + 2*	1.0 × 10 ¹³	34.12
R(15) NO + * → NO*	1.0	0.00
R(16) NO* → NO + *	1.0 × 10 ¹³	71.40
R(17) NO ₂ + * → NO ₂ *	1.0	0.00
R(18) NO ₂ * → NO ₂ + *	1.0 × 10 ¹³	79.38
R(19) NO ₃ + * → NO ₃ *	1.0	0.00
R(20) NO ₃ * → NO ₃ + *	1.0 × 10 ¹³	206.15
R(21) CH ₃ CO + * → CH ₃ CO*	1.0	0.00
R(22) CH ₃ CO* → CH ₃ CO + *	1.0 × 10 ¹³	98.80
R(23) CH ₃ COO + * → CH ₃ COO*	1.0	0.00
R(24) CH ₃ COO* → CH ₃ COO + *	1.0 × 10 ¹³	148.72
R(25) OH + * → OH*	1.0	0.00
R(26) OH* → OH + *	1.0 × 10 ¹³	251.46
R(27) CO + * → CO*	1.0	0.00
R(28) CO* → CO + *	1.0 × 10 ¹³	56.69
R(29) C ₃ H ₇ O + * → C ₃ H ₇ O*	1.0	0.00
R(30) C ₃ H ₇ O* → C ₃ H ₇ O + *	1.0 × 10 ¹³	155.54
R(31) CH ₃ O + * → CH ₃ O*	1.0	0.00
R(32) CH ₃ O* → CH ₃ O + *	1.0 × 10 ¹³	149.87
R(33) HCO + * → HCO*	1.0	0.00
R(34) HCO* → HCO + *	1.0 × 10 ¹³	104.16
R(35) C ₃ H ₇ OH + * → C ₃ H ₇ OH*	1.0	0.00
R(36) C ₃ H ₇ OH* → C ₃ H ₇ OH + *	1.0 × 10 ¹³	39.22
R(37) CH ₃ NO ₂ + * → CH ₃ NO ₂ *	1.0	0.00
R(38) CH ₃ NO ₂ * → CH ₃ NO ₂ + *	1.0 × 10 ¹³	43.71
R(39) CH ₂ NO ₂ + * → CH ₂ NO ₂ *	1.0	0.00
R(40) CH ₂ NO ₂ * → CH ₂ NO ₂ + *	1.0 × 10 ¹³	102.51
R(41) CH ₂ NO + * → CH ₂ NO*	1.0	0.00
R(42) CH ₂ NO* → CH ₂ NO + *	1.0 × 10 ¹³	101.33
R(43) CN + * → CN*	1.0	0.00
R(44) CN* → CN + *	1.0 × 10 ¹³	175.88
R(45) CNO + * → CNO*	1.0	0.00
R(46) CNO* → CNO + *	1.0 × 10 ¹³	199.16
R(47) NCO + * → NCO*	1.0	0.00
R(48) NCO* → NCO + *	1.0 × 10 ¹³	196.23
R(49) NO + O* → NO ₂ * + *	1.0 × 10 ¹¹	39.15
R(50) NO ₂ * + * → NO + O*	1.0 × 10 ¹¹	19.70
R(51) NO ₂ * + O* → NO ₃ * + *	1.0 × 10 ¹¹	31.68
R(52) NO ₃ * + * → NO ₂ + O*	1.0 × 10 ¹¹	32.48
R(53) C ₃ H ₈ * + O* → C ₃ H ₇ OH* + *	1.0 × 10 ¹¹	0.00
R(54) C ₃ H ₇ OH* + * → C ₃ H ₈ * + O*	1.0 × 10 ¹¹	81.42
R(55) C ₃ H ₇ OH* + O* → C ₃ H ₇ O* + OH*	1.0 × 10 ¹¹	37.60
R(56) C ₃ H ₇ O* + OH* → C ₃ H ₇ OH* + O*	1.0 × 10 ¹¹	58.50
R(57) C ₃ H ₇ O* + O* → CH ₃ CHO* + CH ₃ O*	1.0 × 10 ¹¹	9.75
R(58) CH ₃ CHO* + CH ₃ O* → C ₃ H ₇ O* + O*	1.0 × 10 ¹¹	96.45
R(59) CH ₃ CHO* + O* → CH ₃ CO* + OH*	1.0 × 10 ¹¹	4.92
R(60) CH ₃ CO* + OH* → CH ₃ CHO* + O*	1.0 × 10 ¹¹	33.38
R(61) CH ₃ CO* + O* → CH ₃ O* + CO*	1.0 × 10 ¹¹	0.00
R(62) CH ₃ O* + CO* → CH ₃ CO* + O*	1.0 × 10 ¹¹	139.28
R(63) CH ₃ O* + O* → HCO* + H ₂ O*	1.0 × 10 ¹¹	8.42
R(64) HCO* + H ₂ O* → CH ₃ O* + O*	1.0 × 10 ¹¹	95.10
R(65) HCO* + O* → CO ₂ * + H*	1.0 × 10 ¹¹	0.00
R(66) CO ₂ * + H* → HCO* + O*	1.0 × 10 ¹¹	259.57
R(67) CO* + OH* → CO ₂ * + H*	1.0 × 10 ¹¹	10.53
R(68) CO ₂ * + H* → CO* + OH*	1.0 × 10 ¹¹	35.72
R(69) OH* + H* → H ₂ O* + *	1.0 × 10 ¹¹	26.40
R(70) H ₂ O* + * → OH* + H*	1.0 × 10 ¹¹	90.24
R(71) OH* + OH* → H ₂ O* + O*	1.0 × 10 ¹¹	95.49
R(72) H ₂ O* + O* → OH* + OH*	1.0 × 10 ¹¹	30.24

Table 3 (Continued)

Reaction	Pre-exponential (s ⁻¹) or sticking coefficient	E _a (kJ/mol)
R(73) CH ₃ CHO* + O* → CH ₃ COO* + H*	1.0 × 10 ¹¹	2.54
R(74) CH ₃ COO* + H* → CH ₃ CHO* + O*	1.0 × 10 ¹¹	35.76
R(75) CH ₃ COO* + * → CH ₃ O* + CO*	1.0 × 10 ¹¹	17.84
R(76) CH ₃ O* + CO* → CH ₃ COO* + *	1.0 × 10 ¹¹	23.29
R(77) CH ₃ COO* + NO ₂ * → CH ₃ NO ₂ * + CO ₂ *	1.0 × 10 ¹¹	0.00
R(78) CH ₃ NO ₂ * + CO ₂ * → CH ₃ COO* + NO ₂ *	1.0 × 10 ¹¹	150.22
R(79) CH ₃ CO* + NO ₃ * → CH ₃ NO ₂ * + CO ₂ *	1.0 × 10 ¹¹	0.00
R(80) CH ₃ NO ₂ * + CO ₂ * → CH ₃ CO* + NO ₃ *	1.0 × 10 ¹¹	283.25
R(81) CH ₃ NO ₂ * + O* → CH ₂ NO ₂ * + OH*	1.0 × 10 ¹¹	20.29
R(82) CH ₂ NO ₂ * + OH* → CH ₃ NO ₂ * + O*	1.0 × 10 ¹¹	18.37
R(83) CH ₂ NO ₂ * + * → CH ₂ NO* + O*	1.0 × 10 ¹¹	17.64
R(84) CH ₂ NO* + O* → CH ₂ NO ₂ * + *	1.0 × 10 ¹¹	60.14
R(85) CH ₂ NO* + O* → CNO* + H ₂ O*	1.0 × 10 ¹¹	0.00
R(86) CNO* + H ₂ O* → CH ₂ NO* + O*	1.0 × 10 ¹¹	123.78
R(87) CNO* + * → CN* + O*	1.0 × 10 ¹¹	84.68
R(88) CN* + O* → CNO* + *	1.0 × 10 ¹¹	30.62
R(89) CN* + O* → NCO* + *	1.0 × 10 ¹¹	0.00
R(90) NCO* + * → CN* + O*	1.0 × 10 ¹¹	242.34
R(91) NCO* + O* → N* + CO ₂ *	1.0 × 10 ¹¹	0.00
R(92) N* + CO ₂ * → NCO* + O*	1.0 × 10 ¹¹	202.80
R(93) NCO* + * → N* + CO*	1.0 × 10 ¹¹	0.69
R(94) N* + CO* → NCO* + *	1.0 × 10 ¹¹	49.23

4. Numerical modelling

4.1. Assumptions

An automotive monolith consists of hundreds of parallel channels. Each channel within the monolith shares the same behaviour, in terms of transport and chemical properties and velocity, temperature and concentration profiles, so a single channel can represent the whole matrix. While the square cross-section channel is rounded by the washcoat at corners of channel, the single channel can be modelled in two dimensions by considering the channel tubular. Due to no temperature gradient between individual channels, the single channel is considered an adiabatic condition. Usually the automotive monolith is made from low heat conduction material, ceramic in general; as a result thermal conduction in walls is negligible. In after treatment applications, since temperature is moderately high and small residence times of the exhaust gas within the monolith for common operating conditions, homogeneous gas phase reaction is neglected. The engine exhaust is assumed to be ideal gas because it is not only moderately high

Table 4

Optimised pre-exponentials or sticking coefficient of important elementary reactions that dramatically affect optimisation targets.

Active parameter	Sticking coefficient or Pre-exponential factor (s ⁻¹) value
S ₁₅ ⁰	0.9837
A ₁₆	3.16 × 10 ¹⁴
A ₅₅	−3.98 × 10 ¹² T _s + 7.58 × 10 ¹² when T _{in} ≤ 563.15 K −2.34 × 10 ¹¹ T _s + 5.39 × 10 ¹¹ when T _{in} > 563.15 K
A ₅₉	9.13 × 10 ³ e ^{8.63T_s}
A ₆₇	9.46 × 10 ⁵ T _s ² + 3.63 × 10 ⁵ THC _s ² − 2.27 × 10 ⁴ NO _s ² + 2.32 × 10 ⁴ T _s THC _s + 8.35 × 10 ⁵ T _s NO _s 5.48 × 10 ⁴ THC _s NO _s − 5.23 × 10 ⁵ T _s − 1.39 × 10 ⁶ THC _s − 1.35 × 10 ⁶ NO _s + 5 × 10 ⁵
A ₇₃	5.88 × 10 ¹⁵ e ^{−4.32T_s}
A ₇₅	6.84 × 10 ¹¹ T _s ^{−9.7702} e ^{−0.0545(THC/NO)_{in}}
A ₇₇	2.53 × 10 ¹¹ T _s ² − 1.31 × 10 ¹² T _s + 1.85 × 10 ¹²
A ₉₁	2.88 × 10 ⁹ T _s ² + 2.08 × 10 ¹⁰ T _s − 2.57 × 10 ¹⁰

S⁰ is the sticking coefficient and A is the preexponential factor. T_s = T_{inlet}/300, THC_s = THC_{inlet}/1000, NO_s = NO_{inlet}/100. T_{inlet} in the unit of Kelvin, THC_{inlet} and NO_{inlet} in the unit of ppm.

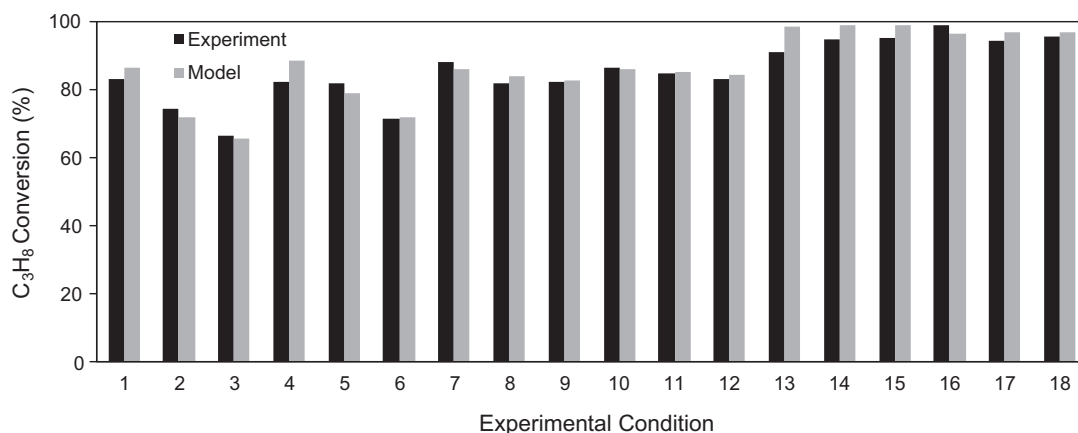


Fig. 3. Comparisons between model predictions and experimental data for the conversion of C₃H₈ at various operating conditions.

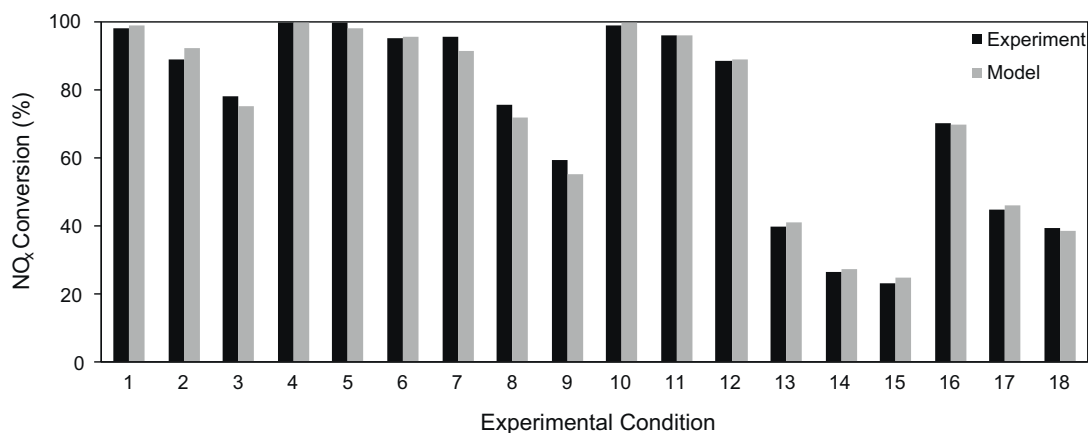


Fig. 4. Comparisons between model predictions and experimental data for the conversion of NO_x at various operating conditions.

temperature but also low pressure, close to atmospheric. Normally Reynolds number based on channel diameter and inlet flow condition in after treatment system does not exceed 2300; thus flow is laminar.

4.2. Governing equations

A governing equation is a system of mathematical equations which describes the relationship among the physical and chemical properties controlling the behaviour of a process. In catalytic reaction fields, these equations are established from the

conservation laws of mass, momentum, species and energy as well as physical and chemical property relationships. These equations are written in the form of a cylindrical spatial coordinate for steady state conditions [46].

4.3. Boundary conditions

The flow enters the computational domain with known velocities, gas compositions and temperatures. A uniform axial velocity of 0.6 m/s and a zero radial velocity are specified at inlet boundary. At the exit of computational domain, an outlet boundary is set

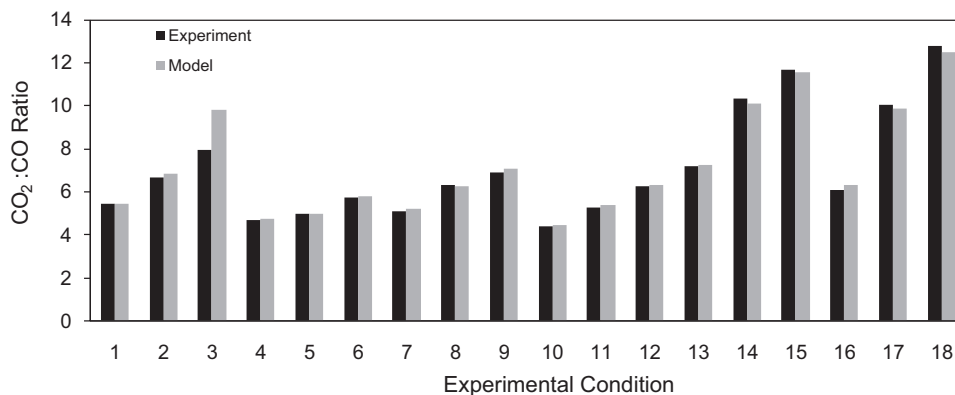


Fig. 5. Comparisons between model predictions and experimental data for the ratio of CO₂ to CO at various operating conditions. Experimental conditions are given in Table 2.

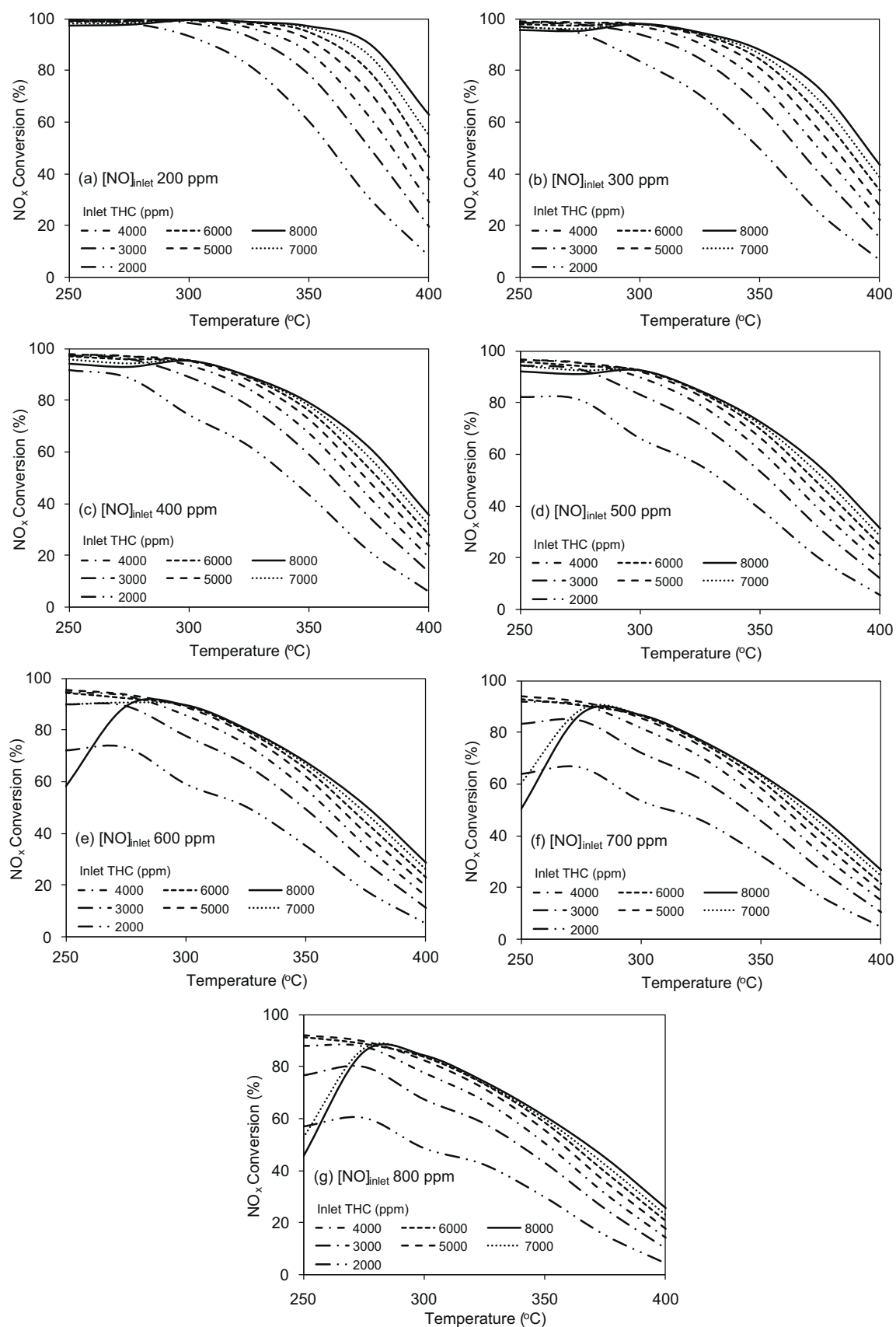


Fig. 6. Model prediction of NO_x conversion as a function of temperature at different inlet concentration of C_3H_8 and NO .

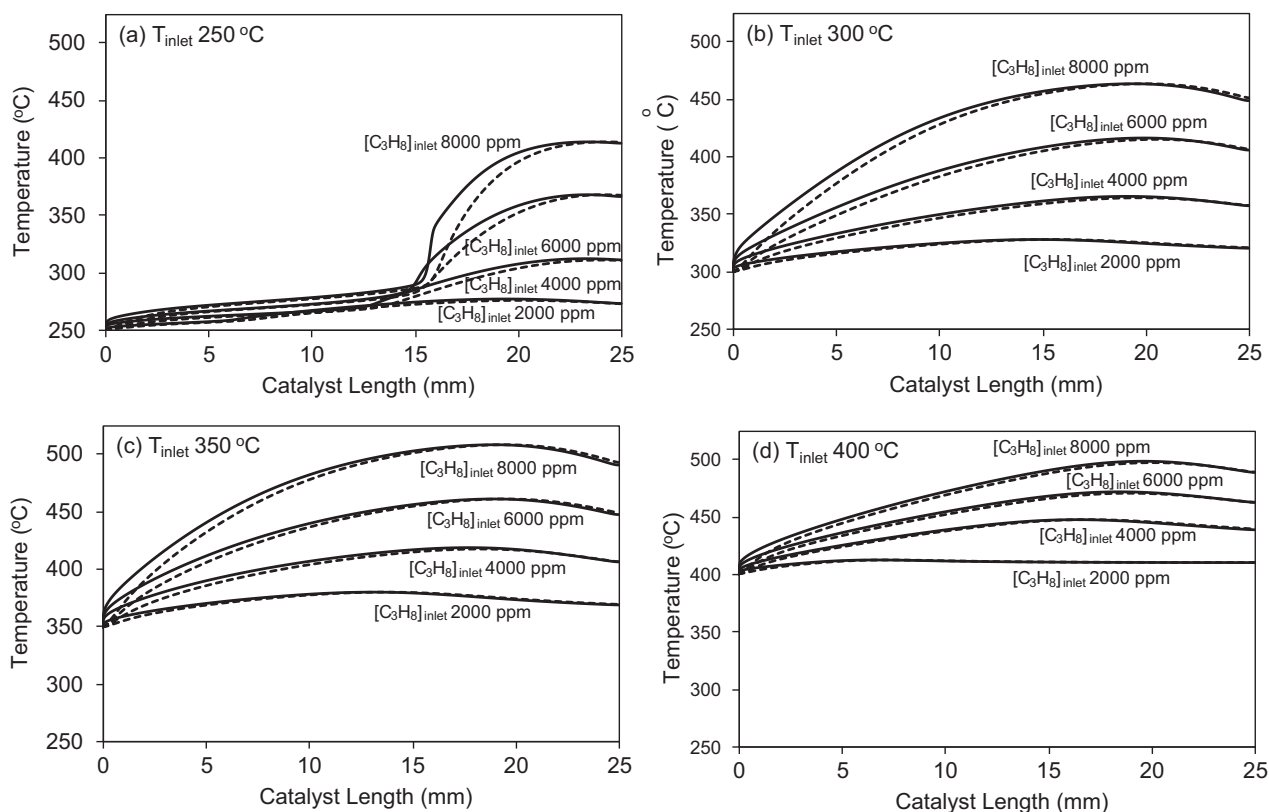


Fig. 7. Wall (Solid lines) and axial gas (dashed lines) temperature profiles; operating condition: 400 ppm of NO.

by atmospheric pressure. At the channel centreline, a symmetry boundary condition is applied. The boundary condition at wall is the most important part in the application of heterogeneous combustion simulation. A detailed multi-step reaction mechanism based on microkinetic analysis as shown in Table 3 is applied at wall boundary in order to model the surface chemistry occurring on the catalyst surface.

5. Results and discussion

5.1. Validation

The validations between model predictions and experimental data are displayed in Figs. 3–5. The conversions of C_3H_8 and NO_x are defined as:

$$C_3H_8 \text{ conversion (\%)} = \frac{[CO]_{outlet} + [CO_2]_{outlet}}{[THC]_{inlet}} \times 100$$

$$NO_x \text{ conversion (\%)} = \frac{([NO] + [NO_2])_{inlet} - ([NO] + [NO_2])_{outlet}}{([NO] + [NO_2])_{inlet}} \times 100$$

Comparisons of model predictions and data from experiments for the C_3H_8 conversion displayed in Fig. 3 show that simulations can predict the experimental results accurately. Propane conversion increases directly with temperatures. Interestingly, at relatively low temperature or approximately 250 °C, the C_3H_8 conversion decrease obviously as the concentration of input NO rise. In contrast, at relative medium and high temperature, 290 and 370 °C, the quantities of input NO slightly affect the C_3H_8 conversions.

NO_x conversions declined noticeably when the NO concentration was increased, with experimental condition (1–3), (4–6), (7–9),

(10–12), (13–15) and (16–18). In HC-SCR, the input hydrocarbon is consumed by two chemical processes: complete oxidation and selective reduction of NO_x . Insufficient hydrocarbon concentration (approximately 2000 ppm of C_3H_8) led to the reduced conversion of NO_x .

At the approximately equal quantity of input C_3H_8 and NO (experimental condition (1,7,13), (2,8,14), (3,9,15), (4,10,16), (5,11,17) and (6,12,18)), NO_x conversion dropped when the operating temperature was increased. This indicates that at these temperatures, hydrocarbons are predominantly preferable to completely oxidise with oxygen rather than selectively reduce with NO_x .

Validations displayed in Fig. 5 show that CO_2 to CO ratios from a range of experimental conditions can be predicted by simulation. At the same input C_3H_8 and temperature condition, the graph clearly show that CO_2 to CO ratios increase directly with concentrations of NO. This implies that the creation of CO_2 relates kinetically to the input concentration of NO. From Table 3, species derived from NO, such as NO_2 , NO_3 and NCO, can be linked to CO_2 through R(77), R(79) and R(91). Due to low activation energy, these elementary reactions can occur easily to produce CO_2 . Therefore, more inlet NO concentration results in more CO_2 production.

5.2. Simulations of C_3H_8 -SCR on a silver catalyst

The effects of temperature, C_3H_8 and NO on NO_x conversions are shown in Fig. 6. Regardless the inlet concentration of C_3H_8 and NO, conversions of NO_x reduce visibly when inlet temperatures increase. At relatively high temperatures, propane which is used as a reducing agent prefers to directly oxidise with oxygen. Fig. 6 can be used to suggest the suitable quantity of propane when the other operating conditions (temperature and NO_x concentration) are known. For example, at temperature of 400 °C, the NO_x

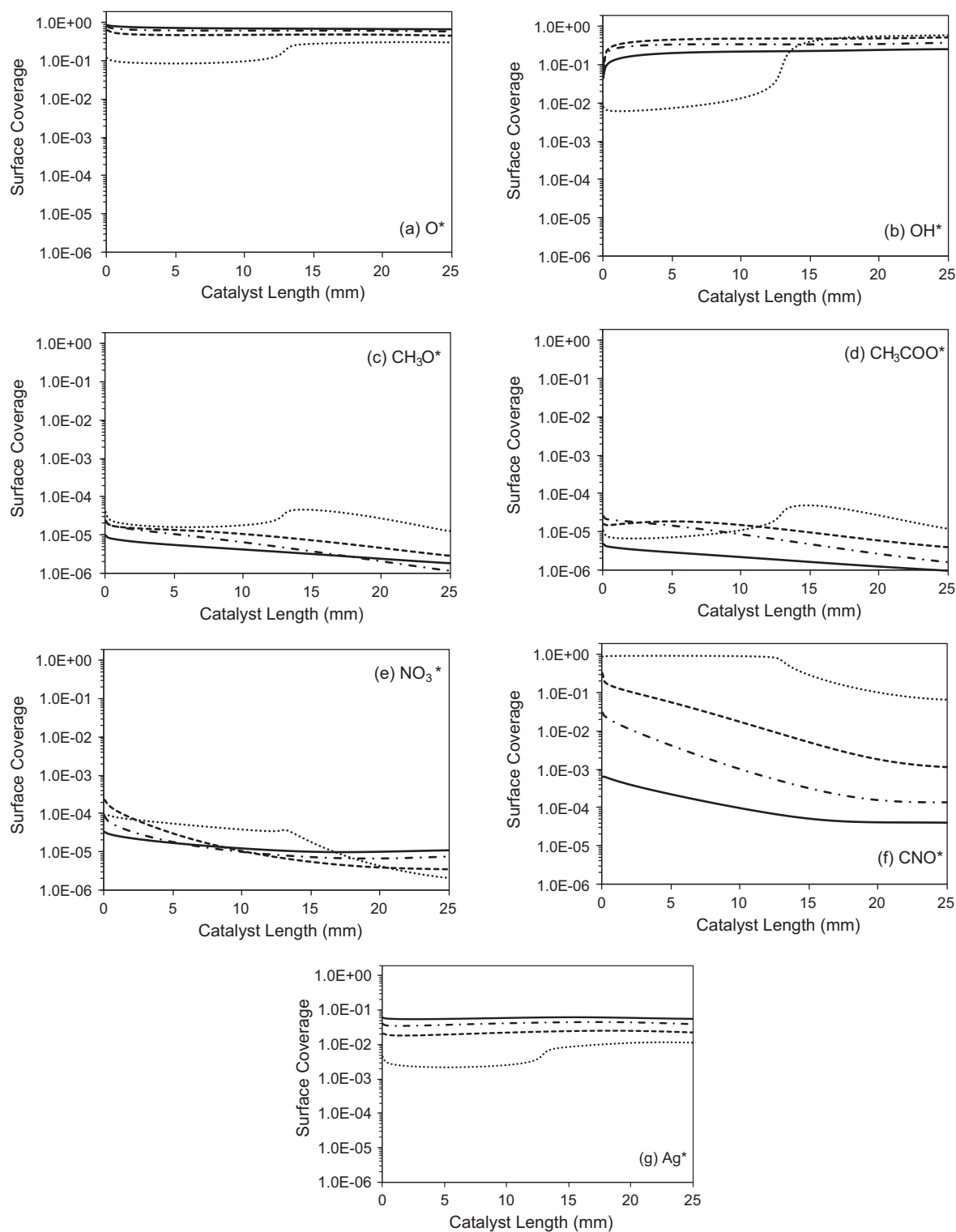


Fig. 8. Simulated surface coverage profiles of surface species, O, OH, CH_3O , CH_3COO , NO_3 , CNO and Ag; the dotted, dashed, dot dashed and solid lines stand for inlet temperature 250, 300, 350 and 400 °C respectively; operating condition: 4000 ppm THC of C_3H_8 and 400 ppm of NO.

conversion is higher than 40% only when THC to NO ratio is higher than 25 (Fig. 6(a) and (b)).

Wall and axial temperatures for different inlet temperatures and inlet concentrations of C_3H_8 are presented in Fig. 7. The wall temperatures are predicted to be higher than the axial temperatures for all operating conditions; consequently, the C_3H_8 -SCR process can be reasonably defined as an exothermic reaction. When

the concentration of the input propane is increased, there are more hydrocarbons to react with oxygen (complete oxidation) and NO_x (selective reduction); so both wall and axial temperatures increase as well. In contrast, a change of the inlet NO concentration slightly affects both wall and axial temperatures (the results are not shown). Interestingly, at 250 °C inlet temperature (Fig. 7(a)), wall and axial temperatures rise gradually by approximately 25 °C;

then the temperatures are sharply increase. This motivating situation can lead to the hypothesis that the C_3H_8 -SCR based on a silver catalyst with promotion of H_2 initiates at approximately 270–280 °C. Furthermore, Fig. 7(a) also show that the temperature steep increase starts at roughly 15 mm. This means that the first approximately 15 mm part of the catalyst is not used for C_3H_8 -SCR, and can be called inactive length. The inadequate catalytic surface (as a result of the inactive length) on NO_x conversions can be perceptibly seen especially at operating conditions that more active surface is required to convert input NO_x (low temperatures and high inlet concentrations of C_3H_8 and NO , Fig. 6(e)–(g)). At these operating conditions, NO_x conversion is obviously low.

Catalyst surface coverage by major species (i.e. atomic oxygen, hydroxyl, methoxy radical, acetate, nitrate and nitrile N-oxide) is presented in Fig. 8. The reason of the inactive catalyst length at relatively low temperature, 250 °C, can be explained in Fig. 8(f), almost the entire catalyst surface is covered by nitrile N-oxide (CNO). As a result, there are not enough active sites for other gas species to adsorb on. From R(87) in Table 3, the relatively high activation energy, 84.68 kJ/mol, is required to transform surface nitrile N-oxide to surface cyanide and atomic oxygen. Thus it can be concluded that at relatively low temperature, 250 °C, the transformation of surface nitrile N-oxide to surface cyanide is the rate determining step and the surface nitrile N-oxide is the most abundant reaction intermediate. After the temperature that SCR processes are initiated, approximately 270–280 °C, surface nitrile N-oxide decrease rapidly. Accordingly, active sites not occupied by nitrile N-oxide are more available to activate other chemical reaction steps. These steps include the formations of surface atomic oxygen, hydroxyl, methoxy radical and acetate as the sudden increases of these surface species are obviously observed. At temperature from 300 to 400 °C, the main surface species are atomic oxygen and hydroxyl. These abundant surface intermediates are in agreement with the recent paper published by Mhadeshwar et al. [39]. From Table 3, relatively high activation energies are required for the desorption of surface hydroxyl, 251.46 kJ/mol in R(26), and the formation of surface water from surface hydroxyls, 95.49 kJ/mol in R(71). This explains the fact that surface hydroxyl still remains as the major species on the active sites. The large amount of oxygen (usually found in exhaust from diesel engines) as well as a medium activation energy for its desorption process, 39.55 kJ/mol in R(8), make atomic oxygen the main surface species as well.

The effect of temperatures on the surface coverage of predominant surface species is demonstrated in Fig. 9. Values of surface coverage are taken at the outlet of the channel. The figure proves that atomic oxygen and hydroxyl are the most abundant reaction intermediate throughout the range of inlet temperature. The surface hydroxyl tends to decrease gradually when the inlet temperature is risen. Earlier it was explained that high activation energies so needed high temperature to react, the rate of depletion of surface hydroxyl, R(26) and R(71), is promoted when the temperature is increased. In contrast with the surface hydroxyl, surface atomic oxygen increases steadily as a function of inlet temperatures. An excessive amount of oxygen (usually found in the exhaust from lean burn engine) makes the atomic oxygen the principal species depositing on the surface of catalyst. A growth in surface coverage of surface NO, NO_2 and NO_3 with temperature is the result of the insufficiency of hydrocarbon to selectively reduce these surface species at high temperature conditions. Vacant sites, Ag^* , increase with temperature as a result from less occupation on active sites of surface species, especially hydroxyl. Moreover, the surface coverage of NO_3 is obviously higher than that of NO and NO_2 . This simulation result coincides with the study by Kameoka et al. [25] as previously mentioned that adsorbed NO and NO_2 were hardly observed on the surface of catalyst.

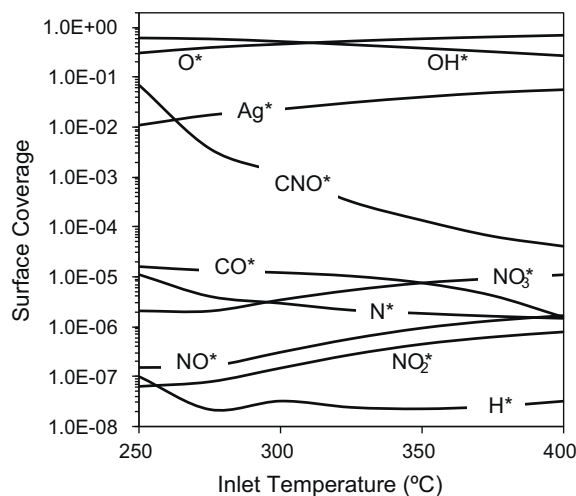


Fig. 9. Simulated surface coverages of different surface species as a function of temperature; value taken at channel outlet; operating condition: 4000 ppm THC of C_3H_8 and 400 ppm of NO.

6. Conclusions

Silver-alumina based catalyst is a promising candidate for practical uses of selective catalytic reduction of NO_x by hydrocarbons. To develop highly efficient HC-SCR systems, a detailed understanding in terms of both physical and chemical phenomena is required. This requirement can be effectively accomplished by using computerised simulation rooted in computational fluid dynamics (CFD) and a detailed elementary reaction mechanism. Information on kinetic processes of HC-SCR on silver based catalysts, such as intermediate species and reaction pathways, was carefully taken from available literature. Microkinetic analysis was systematically applied in order to elucidate the chemical phenomena that took place on the catalyst surface. Instead of fitting from experimental data, rate parameters appearing in the detailed elementary reactions were initially estimated by using theory of chemical bonding, TST and UBI-QEP. Initial rate parameters were optimised by using sensitivity analysis and solution-mapping method. Sensitivity analysis was used to find the most important elementary reactions. The solution-mapping method was subsequently employed to determine an optimum set of pre-exponential factors. These pre-exponential factors were fitted in the polynomial form as a function of inlet temperatures and concentrations.

Numerical simulations of C_3H_8 -SCR in a single channel of the silver based catalyst were validated with experimental data. At different inlet temperatures and concentrations, the comparisons were shown that the conversions of C_3H_8 and NO_x as well as the ratios of CO_2 to CO that were predicted by modelling agreed very well with data from experiments. The numerical simulation can predict the effect on the NO_x conversion of operating conditions, for instance, inlet concentration of C_3H_8 and NO_x and inlet temperature. Furthermore, because of the small scale of individual channels, numerical simulation can provide both physical and chemical data that are difficult or impractical to measure, for example, concentration and temperature profiles, wall temperatures and surface coverages. Finally, computational modelling can be used as an effective tool to aid development of an optimal after treatment system.

Acknowledgements

Support for this work by the Engineering and Physical Science Research Council (EPSRC) and Johnson Matthey Plc is gratefully

acknowledged. The Royal Thai Government is also acknowledged for the provision of the PhD scholarship and maintenance grant to Mr. Boonlue Sawatmongkhon.

Appendix A.

A.1. Governing equations

Conservation of total mass or continuity equation

$$\frac{\partial}{\partial z}(\rho v_z) + \frac{1}{r} \frac{\partial}{\partial r}(r \rho v_r) = 0$$

Axial momentum equation

$$\rho v_z \frac{\partial v_z}{\partial z} + \rho v_r \frac{\partial v_z}{\partial r} = -\frac{\partial P}{\partial z} + \frac{\partial}{\partial z} \left[2\mu \frac{\partial v_z}{\partial z} - \frac{2}{3} \mu \left(\frac{\partial v_z}{\partial z} + \frac{1}{r} \frac{\partial(r v_r)}{\partial r} \right) \right] + \frac{1}{r} \frac{\partial}{\partial r} \left[\mu r \left(\frac{\partial v_r}{\partial z} + \frac{\partial v_z}{\partial r} \right) \right]$$

Radial momentum equation

$$\rho v_z \frac{\partial v_r}{\partial z} + \rho v_r \frac{\partial v_r}{\partial r} = -\frac{\partial P}{\partial r} + \frac{\partial}{\partial z} \left[\mu \left(\frac{\partial v_r}{\partial z} + \frac{\partial v_z}{\partial r} \right) \right] + \frac{\partial}{\partial r} \left[2\mu \frac{\partial v_r}{\partial r} - \frac{2}{3} \mu \left(\frac{\partial v_z}{\partial z} + \frac{1}{r} \frac{\partial(r v_r)}{\partial r} \right) \right] + \frac{2\mu}{r} \left[\frac{\partial v_r}{\partial r} - \frac{v_r}{r} \right]$$

Conservation of species or species continuity equation

$$\rho v_z \frac{\partial Y_i}{\partial z} + \rho v_r \frac{\partial Y_i}{\partial r} = -\frac{\partial J_{i,z}}{\partial z} + \frac{1}{r} \frac{\partial(r J_{i,r})}{\partial r} + R_i \quad (i = 1, \dots, N_g)$$

Conservation of energy

$$\rho C_p \left(v_z \frac{\partial T}{\partial z} + v_r \frac{\partial T}{\partial r} \right) = \left(v_z \frac{\partial P}{\partial z} + v_r \frac{\partial P}{\partial r} \right) + \frac{\partial}{\partial z} \left(\lambda \frac{\partial T}{\partial z} \right) + \frac{\partial}{\partial r} \left(r \lambda \frac{\partial T}{\partial r} \right) - \sum_{i=1}^{N_g} C_{p,i} \left(J_{i,z} \frac{\partial T}{\partial z} + J_{i,r} \frac{\partial T}{\partial r} \right) - \sum_{i=1}^{N_g} h_i R_i$$

Diffusive mass flux

$$J_{i,z} = -\rho D_{i,B} \frac{\partial Y_i}{\partial z}$$

$$J_{i,r} = -\rho D_{i,B} \frac{\partial Y_i}{\partial r}$$

In these equations the independent variables are the axial and radial coordinates, z and r respectively. The dependent variables that are solved by these equations are: axial velocity (v_z), radial velocity (v_r), mass fraction of species i (Y_i), temperature (T) and static pressure (P). Other variables that are determined by auxiliary equations are: mass density (ρ), viscosity (μ) thermal conductivity (λ), specific heat (C_p), enthalpy of species i (h_i), net rate of production of species i due to chemical reactions (R_i), diffusive mass flux of species i in axial direction ($J_{i,z}$), diffusive mass flux of species i in radial direction ($J_{i,r}$) and molecular diffusion coefficient of species i diffusing in the mixture of i and B ($D_{i,B}$). Here N_g is the number of gas phase species. The mass density is calculated by using the equation of state. The viscosity and the thermal conductivity of the mixture are computed via the kinetic theory. The molecular diffusion coefficients are estimated by the method of Fuller, Schettler and Giddings [47].

A.2. Boundary conditions

$$J_{i,r=R} = \dot{s}_i M_i$$

$$\dot{s}_i = \sum_{k=1}^{K_s} (v''_{i,k} - v'_{i,k}) k_k \prod_{j=1}^{N_g+N_s} c_j^{v'_{j,k}}, \quad (i = 1, \dots, N_g + N_s)$$

Here, \dot{s}_i is surface reaction rate of species i , M_i is the molecular weight of species i , K_s is the number of elementary reactions, v' (reactants) and v'' (products) are the stoichiometric coefficients, N_s is the number of surface species and c_j is the molecular concentration of species j . The rate coefficients of elementary reaction k , k_k , are defined as an Arrhenius expression:

$$k_k = A_k T^{\beta_k} e^{-\left(\frac{E_{a,k}}{RT}\right)}$$

At this point, A_k , β_k and $E_{a,k}$ are pre-exponential factor, temperature exponent and activation energy for elementary reaction k , respectively. For adsorption processes, the rate coefficients of elementary adsorption reaction k can be written in the form of:

$$k_k = \frac{S_i^0}{\Gamma^n} \sqrt{\frac{RT}{2\pi M_i}}$$

At this time, S_i^0 is sticking coefficient at vanishing coverage of species i , Γ is site density and n is reaction order.

References

- [1] V. Tufano, M. Turco, Appl. Catal. B: Environ. 2 (1993) 9–26.
- [2] R.E. Hayes, S.T. Kolaczowski, P.K.C. Li, S. Awdry, Chem. Eng. Sci. 56 (2001) 4815–4835.
- [3] J.A. Dumesic, D.F. Rudd, L.M. Aparicio, J.E. Rekoske, A.A. Treviño, The Microkinetics of Heterogeneous Catalysis, American Chemical Society, Washington DC, 1993.
- [4] X. Zhang, H. He, Z. Ma, Catal. Commun. 8 (2007) 187–192.
- [5] K.-I. Shimizu, M. Tsuzuki, A. Satsuma, Appl. Catal. B: Environ. 71 (2007) 80–84.
- [6] K.-I. Shimizu, H. Kawabata, A. Satsuma, T. Hattori, J. Phys. Chem. B 103 (1999) 5240–5245.
- [7] K.-I. Shimizu, J. Shibata, A. Satsuma, T. Hattori, Phys. Chem. Chem. Phys. 3 (2001) 880–884.
- [8] K. Arve, H. Backman, F. Klingstedt, K. Eränen, D.Y. Murzin, Appl. Catal. B: Environ. 70 (2007) 65–72.
- [9] V. Houel, P. Millington, R. Rajaram, A. Tsolakis, Appl. Catal. B: Environ. 77 (2007) 29–34.
- [10] K.-I. Shimizu, A. Satsuma, T. Hattori, Appl. Catal. B: Environ. 25 (2000) 239–247.
- [11] V. Houel, P. Millington, R. Rajaram, A. Tsolakis, Appl. Catal. B: Environ. 73 (2007) 203–207.
- [12] S. Satokawa, J. Shibata, K.-I. Shimizu, A. Satsuma, T. Hattori, Appl. Catal. B: Environ. 42 (2003) 179–186.
- [13] J. Shibata, K.-I. Shimizu, S. Satokawa, A. Satsuma, T. Hattori, Phys. Chem. Chem. Phys. 5 (2003) 2154–2160.
- [14] P. Sazama, L. Capek, H. Drobná, Z. Sobalík, J. Dedecek, K. Arve, B. Wichterlová, J. Catal. 232 (2005) 302–317.
- [15] K.-I. Shimizu, J. Shibata, A. Satsuma, J. Catal. 239 (2006) 402–409.
- [16] D. Creaser, H. Kannisto, J. Sjöblom, H.H. Ingelsten, Appl. Catal. B: Environ. 90 (2009) 18–28.
- [17] X. Zhang, Y. Yu, H. He, Appl. Catal. B: Environ. 76 (2007) 241–247.
- [18] B. Wichterlová, P. Sazama, J.P. Breen, R. Burch, C.J. Hill, L. Capek, Z. Sobalík, J. Catal. 235 (2005) 195–200.
- [19] A.B. Mhadeshwar, D.G. Vlachos, J. Catal. 234 (2005) 48–63.
- [20] E. Shustorovich, H. Sellers, Surf. Sci. Rep. 31 (1998) 1–119.
- [21] H. Sellers, E. Shustorovich, Surf. Sci. 504 (2002) 167–182.
- [22] E. Shustorovich, A.V. Zeigarnik, Surf. Sci. 527 (2003) 137–148.
- [23] M.M. Bettahar, G. Costentin, L. Savary, J.C. Lavalley, Appl. Catal. A: Gen. 145 (1996) 1–48.
- [24] K.-I. Shimizu, A. Satsuma, Phys. Chem. Chem. Phys. 8 (2006) 2677–2695.
- [25] S. Kameoka, Y. Ukisu, T. Miyadera, Phys. Chem. Chem. Phys. 2 (2000) 367–372.
- [26] K.-I. Shimizu, J. Shibata, H. Yoshida, A. Satsuma, T. Hattori, Appl. Catal. B: Environ. 30 (2001) 151–162.
- [27] T. Chafik, S. Kameoka, Y. Ukisu, T. Miyadera, J. Mol. Catal. A: Chem. 136 (1998) 203–211.
- [28] Y. Yu, H. He, Q. Feng, J. Phys. Chem. B 107 (2003) 13090–13092.
- [29] Y. Yu, H. He, Q. Feng, H. Gao, X. Yang, Appl. Catal. B: Environ. 49 (2004) 159–171.
- [30] Y.H. Yeom, B. Wen, W.M.H. Sachtler, E. Weitz, J. Phys. Chem. B 108 (2004) 5386–5404.
- [31] Y.H. Yeom, M. Li, W.M.H. Sachtler, E. Weitz, J. Catal. 238 (2006) 100–110.
- [32] Y.H. Yeom, M. Li, W.M.H. Sachtler, E. Weitz, J. Catal. 246 (2007) 413–427.
- [33] Y. Yeom, M. Li, A. Savara, W. Sachtler, E. Weitz, Catal. Today 136 (2008) 55–63.
- [34] R. Burch, J.P. Breen, F.C. Meunier, Appl. Catal. B: Environ. 39 (2002) 283–303.

- [35] Y. Yu, X. Zhang, H. He, *Appl. Catal. B: Environ.* 75 (2007) 298–302.
- [36] S. Kameoka, T. Chafik, Y. Ukisu, T. Miyadera, *Catal. Lett.* 55 (1998) 211–215.
- [37] N. Bion, J. Saussey, M. Haneda, M. Daturi, *J. Catal.* 217 (2003) 47–58.
- [38] S. Tamm, H.H. Ingelsten, A.E.C. Palmqvist, *J. Catal.* 255 (2008) 304–312.
- [39] A.B. Mhadeshwar, B.H. Winkler, B. Eiteneer, D. Hancu, *Appl. Catal. B: Environ.* 89 (2009) 229–238.
- [40] Y.-R. Luo, *Comprehensive Handbook of Chemical Bond Energies*, CRC Press, 2007.
- [41] S. Storsæter, D. Chen, A. Holmen, *Surf. Sci.* 600 (2006) 2051–2063.
- [42] M. Frenklach, H. Wang, M.J. Rabinowitz, *Prog. Energy Combust. Sci.* 18 (1992) 47–73.
- [43] P. Aghalayam, Y.K. Park, D.G. Vlachos, *AIChE J.* 46 (2000) 2017–2029.
- [44] J. Koop, O. Deutschmann, *Appl. Catal. B: Environ.* 91 (2009) 47–58.
- [45] A.B. Mhadeshwar, D.G. Vlachos, *J. Phys. Chem. B* 109 (2005) 16819–16835.
- [46] J. Braun, T. Hauber, H. Többen, P. Zacke, D. Chatterjee, O. Deutschmann, J. Warnatz, SAE Paper No. 2000-01-0211 (2000).
- [47] R.C. Reid, J.M. Prausnitz, T.K. Sherwood, *The Properties of Gases and Liquids*, 3rd ed, McGraw-Hill, 1977.